







SHORT REPORT

Open Access



Improved simultaneous mapping of epigenetic features and 3D chromatin structure via ViCAR

Sean M. Flynn^{1†}, Somdutta Dhir^{1†}, Krzysztof Herka^{1†}, Colm Doyle^{1†}, Larry Melidis¹, Angela Simeone¹, Winnie W. I. Hui¹, Rafael de Cesaris Araujo Tavares¹, Stefan Schoenfelder², David Tannahill¹ and Shankar Balasubramanian^{1,3,4*}

[†]Sean M. Flynn, Somdutta Dhir, Krzysztof Herka and Colm Doyle contributed equally to this work.

*Correspondence: sb10031@cam.ac.uk

¹ Cancer Research UK Cambridge Institute, Li Ka Shing Centre, Robinson Way, Cambridge CB2 0RE, UK

² Epigenetics Programme, Babraham Institute, Cambridge CB22 3AT, UK

³ Yusuf Hamied Department of Chemistry, University of Cambridge, Cambridge CB2 1EW, UK

⁴ School of Clinical Medicine, University of Cambridge, Cambridge CB2 0SP, UK

Abstract

Methods to measure chromatin contacts at genomic regions bound by histone modifications or proteins are important tools to investigate chromatin organization. However, such methods do not capture the possible involvement of other epigenomic features such as G-quadruplex DNA secondary structures (G4s). To bridge this gap, we introduce ViCAR (viewpoint HiCAR), for the direct antibody-based capture of chromatin interactions at folded G4s. Through ViCAR, we showcase the first G4-3D interaction landscape. Using histone marks, we also demonstrate how ViCAR improves on earlier approaches yielding increased signal-to-noise. ViCAR is a practical and powerful tool to explore epigenetic marks and 3D genome interactomes.

Keywords: 3D genome structure, Hi-C, Histone marks, G-quadruplex DNA

Background

Chromosome conformation capture methodologies, such as Hi-C [1], provide information on 3D genome structure and function including the role of DNA looping in facilitating enhancer function [2]. Genome-wide Hi-C maps require prohibitively high sequencing depth (often requiring billions of reads), so more pragmatic methods such as Capture Hi-C [3, 4], Hi-C on accessible regulatory DNA (HiCAR) [5], Hi-C Coupled chromatin cleavage and Tagmentation (HiCuT) [6], Proximity Ligation-Assisted ChIP-seq (PLAC-seq) [7], and Hi-C with Chromatin Immunoprecipitation (HiChIP) [8] have been developed to map 3D interactions for specific genome features. For example, HiCAR uses Tn5 transposase activity to tag 3D interactions anchored in accessible genome regions [5].

G-quadruplexes (G4s) are four-stranded structures that can fold in specific G-rich DNA sequences [9, 10]. Folded G4s have been detected in thousands of gene regulatory



© The Author(s) 2024. **Open Access** This article is licensed under a Creative Commons Attribution 4.0 International License, which permits use, sharing, adaptation, distribution and reproduction in any medium or format, as long as you give appropriate credit to the original author(s) and the source, provide a link to the Creative Commons licence, and indicate if changes were made. The images or other third party material in this article are included in the article's Creative Commons licence, unless indicated otherwise in a credit line to the material. If material is not included in the article's Creative Commons licence and your intended use is not permitted by statutory regulation or exceeds the permitted use, you will need to obtain permission directly from the copyright holder. To view a copy of this licence, visit <http://creativecommons.org/licenses/by/4.0/>.

regions in human chromatin [11]. Chromatin immunoprecipitation followed by sequencing (ChIP-seq) [11] and Cleavage Under Targets and Tagmentation (CUT&Tag) [12–16] using G4-specific antibodies or small molecules have generated maps of folded G4 sites in different cell types, states, and diseases. G4s are enriched in active promoters and enhancers, and overlapping these data with independently generated 3D interaction maps suggests that G4s may associate with sites of promoter-enhancer contact [17–20]. Emerging evidence shows that G4 profiles are remodeled to reflect cell identity and transitions between pluripotent and differentiated states, and normal to cancer states [17, 21]. Taken together, these findings suggest that G4s may have a role to play in promoter-enhancer 3D interactions. However, the experimental evidence for the formation of G4s at enhancer-promoter contact sites is not direct and is based on indirect correlations by overlapping independent datasets. A methodology that can detect folded G4 directly at promoter-enhancer interaction sites, in the same DNA fragment (i.e., at read level), would reveal the co-occurrence of G4s at enhancers more convincingly. Herein, we introduce such a method.

Results and discussion

We have developed ViCAR (viewpoint HiCAR) to overcome two major limitations of existing methodologies that are not amenable to mapping G4s directly at 3D contact sites. We aimed to improve (1) the signal-to-noise seen in ChIP-based technologies by deploying CUT&Tag [6, 14, 22] and (2) HiCuT, by enriching ligated fragments, which HiCuT does not do. HiCuT is the only CUT&Tag-based Hi-C method that we know of, but it only has a low proportion of useful reads (cis interactions > 20 kb; Additional file 2: Table S1) [6]. G4 ViCAR works by recruiting Tn5 to folded G4 structures present in chromatin using a G4-specific antibody. Tagmentation is then activated, and subsequent restriction digestion with CviQI followed by ligation connects DNA fragments proximal to the tagmented G4 site. Enrichment of ligation junctions is performed via PCR using one primer that anneals to the mosaic end region of the Tn5 adapter, and another that anneals to a splint oligonucleotide which is ligated to genomic DNA [5] (Fig. 1a). The G4 anchored loop site in the tagmented DNA fragment is then sequenced as Read 2 (R2), while the region that was in spatial proximity is sequenced as Read 1 (Fig. 1a).

To demonstrate the improved efficiency of ViCAR, we first used antibodies for histone marks to provide a comparison with maps of 3D genome structure by HiChIP, PLAC-seq, or HiCuT [6, 23, 24]. We performed ViCAR for the H3K27me3 repressive mark in human embryonic stem cells (hESCs) and mouse embryonic stem cells (mESCs), which captures loops at developmental genes with low levels of expression [25]. Tagmentation of antibody-bound sites was confirmed by the ViCAR R2 signal, which reproducibly enriched H3K27me3 sites as compared to previous hESC (ENCODE) and mESC [26] ChIP-seq data [17] (Fig. 1b–c; Additional file 1: Fig. S1a–d). As expected, ViCAR validated homotypic 3D interactions marked by H3K27me3 on both sides in hESCs [27] (Fig. 1d). Using FitHiChIP [28] to call loops, we identified 161,819 H3K27me3-anchored loops at 5 kb resolution in hESCs (Additional file 1: Fig. S1e–f, Additional file 2: Table S1). Known H3K27me3 loops anchored at HOX clusters and known interchromosomal interactions were clearly exemplified by ViCAR (Additional file 1: Fig. S2a–c) [27]. The improved efficiency of ViCAR was clear from side-by-side comparison

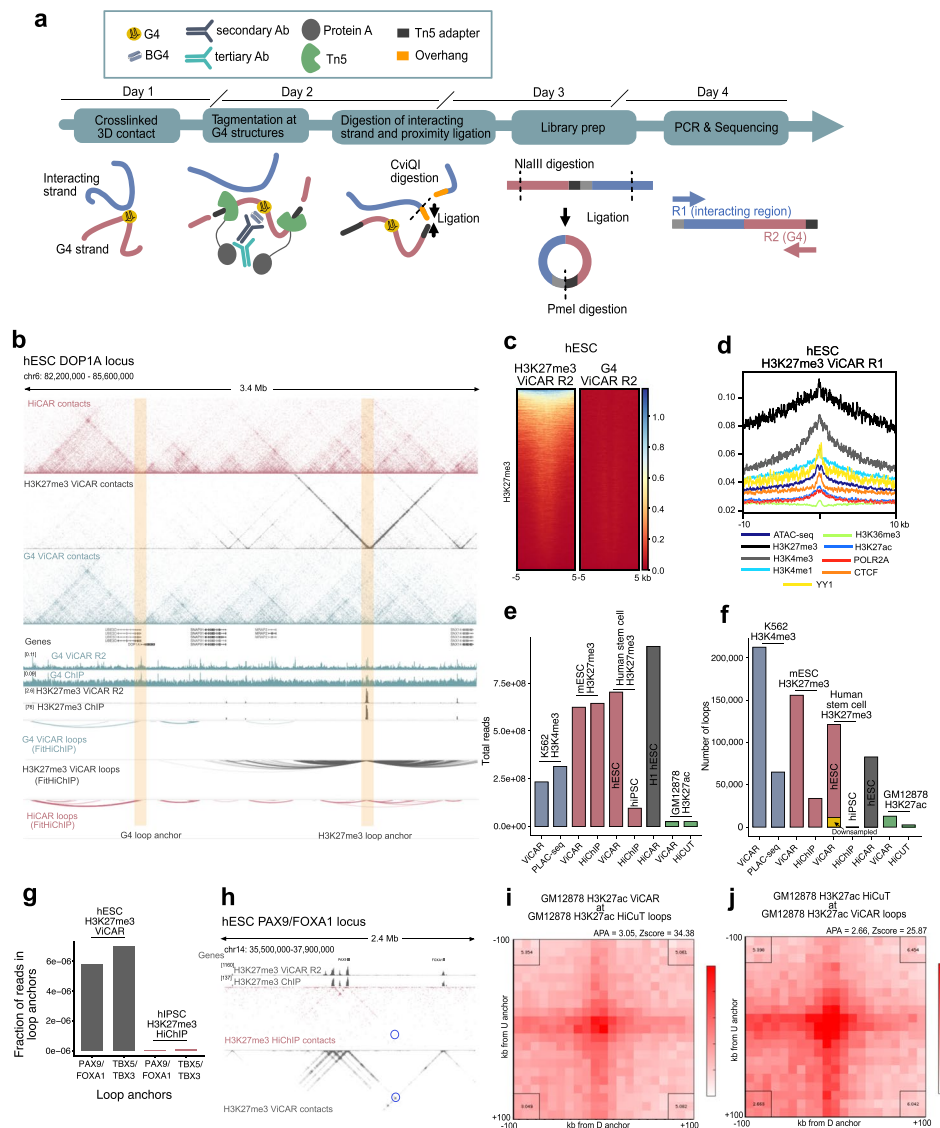


Fig. 1 **a** Overview of the ViCAR method. Tn5 tagments at sites where an antibody binds the desired feature, in this example a folded G4 structure. Subsequently, the genome is digested with CviQ1 and tagmented and digested fragments in spatial proximity ligated. To amplify ligated fragments, an i7 primer that anneals to the Tn5 mosaic end adapter and an i5 primer that anneals to a splint oligonucleotide ligated to genomic DNA are used for PCR. The i7 ends of PCR products are sequenced as R2, and the i5 ends are sequenced as R1. **b** Example locus from ViCAR and HiCAR [5] data for H1 hESCs. Top 3 tracks show raw contact matrices; 2D tracks show ViCAR R2 and ChIP-seq for H3K27me3 and G4s in hESCs. Bottom 3 tracks show significant loops called by FitHiChIP ($q < 0.05$). Highlighted regions are examples of G4- and H3K27me3-centered loop anchors. **c** H3K27me3 ViCAR sequencing R2 plotted over H3K27me3 ChIP-seq peaks (ENCODE) in hESCs (left). G4 ViCAR sequencing R2 over H3K27me3 ChIP-seq peaks is shown for comparison (right). **d** H3K27me3 ViCAR sequencing R1 (i.e., 3D interactions) plotted over ChIP-seq and ATAC-seq peaks. Sequencing depth (**e**) and number of significant loops called by FitHiChIP (**f**) in ViCAR and other methods. The yellow bar in **f** represents hESC H3K27me3 ViCAR data down-sampled to the same number of valid read pairs as the hiPSC H3K27me3 HiChIP data (11,414,395 pairs). **g** and **h** Comparison of hESC H3K27me3 ViCAR and hiPSC H3K27me3 HiChIP data [23] at the PAX9/FOXA1 (chr14: 36,660,000–36,670,000/chr14: 37,590,000–37,600,000) and TBX5/TBX3 (chr12: 114,400,000–114,410,000/chr12: 114,680,000–114,690,000) loci highlighted by Kraft et al. [23]. **g** shows number of reads underlying PAX9/FOXA1 and TBX5/TBX3 loops as a fraction of total number of reads per library. Loops were called by FitHiChIP at 10 kb resolution. **h** shows raw contact matrices for the PAX9/FOXA1 locus. **i** APA plot for GM12878 H3K27ac HiCuT [6] loops using GM12878 H3K27ac ViCAR data. **j** APA plot for GM12878 H3K27ac ViCAR loops using GM12878 H3K27ac HiCuT data [6]

of H3K27me3 ViCAR to H3K27me3 HiChIP data for mESCs and human induced pluripotent stem cells (hiPSCs) [23]. In mESCs, ViCAR identified 284,174 significant loops, whereas published HiChIP [23] only identified 34,597 at a similar sequencing depth. As published HiChIP data from hiPSCs was sequenced to lower depth than ViCAR, for a fair comparison ViCAR data from hESCs was down-sampled to the same number of valid pairs as HiChIP before loop calling. Notably, ViCAR identified 11,433 significant loops, whereas no significant loops were detectable with HiChIP (Fig. 1e–f). On analyzing raw interactions, we found that ViCAR consistently identifies contacts with strikingly improved signal-to-noise compared to HiChIP at the PAX9/FOXA1 and TBX5/TBX3 loci (Fig. 1g–h; Additional file 1: Fig. S2d). Overall, these results demonstrate the improved sensitivity of ViCAR relative to HiChIP for identifying 3D genome interactions.

To further show the advantage of ViCAR over PLAC-seq, we performed ViCAR for the H3K4me3 promoter mark and H3K4me1 enhancer mark in human K562 erythroleukemia cells which have extensive 3D genome maps [24, 29]. We validated ViCAR at the well-characterized MYC locus [24, 29–31], and confirmed that the ViCAR 3D structure was consistent with published in situ Hi-C [29] and PLAC-seq [24] data, and that H3K4me3 ViCAR recovered known MYC promoter-enhancer loops [31] (Additional file 1: Fig. S3a–b). At comparable sequencing depth, ViCAR detects more H3K4me3-anchored loops than PLAC-seq [24] (212,520 vs 65,005; Fig. 1g–h; Additional file 1: Fig. S3c–d; Additional file 2: Table S1). Together, these data show that ViCAR provides increased sensitivity for loop detection compared to HiChIP and PLAC-seq.

To compare ViCAR to HiCuT directly, we performed ViCAR in GM12878 cells using the H3K27ac antibody and down-sampled it to a similar number of reads for published HiCuT H3K27ac data in the same cell type [6] (Additional file 2: Table S1). Whereas in HiCuT data 1.89% of total reads were useful for Hi-C (cis interactions > 20 kb), 30.79% of total reads met the same criteria in ViCAR data (Additional file 2: Table S1). Using FitHiChIP, we identified 12,904 loops with ViCAR, compared to 2639 loops with HiCuT (10 kb resolution, $q < 0.05$; Additional file 2: Table S1). Therefore, ViCAR provides increased sensitivity and represents a significant advance compared to HiCuT.

To further benchmark our method against existing approaches, we confirmed that the size of the loops identified by ViCAR are comparable to those called with HiChIP, PLAC-seq, HiCuT, and HiCAR (Additional file 1: Fig. S4a–h). We also used aggregate peak analysis (APA) [29] to compare enrichment of sites identified by ViCAR and other methods. APA plots showed that HiCuT [6], PLAC-seq [24], and HiChIP [23] loops were enriched in ViCAR data (Fig. 1i and Additional file 1: Fig. S4i–j), suggesting that interactions detected by other methods are also identified by ViCAR. ViCAR loops were also enriched in HiCuT, PLAC-seq, and HiChIP data (Fig. 1j and Additional file 1: Fig. S4k–l) indicating that ViCAR loops are bona fide. Additionally, loops that were unique to H3K4me3 ViCAR were identified in H3K4me3 PLAC-seq upon removal of a q value threshold (Additional file 1: Fig. S4m), supporting this conclusion.

Having established the applicability of ViCAR for histone marks, we next tested the capability of ViCAR to capture additional epigenetic features which have not been directly mapped in 3D genome-wide. To identify loops marked by G4 structures, we performed ViCAR using the G4-specific antibody BG4 in hESCs. Tagmentation near

folded G4 sites was confirmed by the ViCAR R2 signal, which was enriched for G4 sites [17] (Figs. 1b and 2a, Additional file 1: Figs. S1b–c and S5a–b). As suggested by previous associations [17, 18, 20], G4 ViCAR also directly confirmed enrichment of CTCF, YY1, and active histone marks at G4-interacting regions (Fig. 2b). Using FitHiChIP [28] to call loops, we identified 9080 G4 loops at 5 kb resolution in hESCs (Additional file 1: Fig. S1e–f, Additional file 2: Table S1). The majority (>70% with $q < 0.01$) of G4-anchored loops were contained within accessible chromatin HiCAR regions [5] (Additional file 1: Fig. S1e). In contrast, loops anchored by the H3K27me3 repressive mark exhibited little overlap with HiCAR or G4 ViCAR loops (Additional file 1: Fig. S1e–f), demonstrating the depletion of G4s in these regions. Previous comparison of independent ChIP-seq and ChIA-PET (Chromatin Interaction Analysis with Paired-End Tag) data suggests interactions at the KRAS and MDM2 loci [19]. We used ViCAR to directly confirm these G4-3D interactions in K562 cells (Additional file 1: Fig. S5c–d). Overall, our data confirms the existence of G4s at previously predicted sites.

To evaluate whether the G4 ViCAR readout can sense loss of DNA structures in cells, we used CRISPR/Cas9 to remove an endogenous G4 structure in cells. We selected a loop anchor identified above by ViCAR with a short G-rich sequence predicted to form a stable G4. This intronic G4 is located near the regulators of complement activation (RCA) gene cluster. RCA cluster genes including CD55 and CD46 are overexpressed in several malignancies including myeloid leukemia and are a target for cancer therapeutics [32–35], but little is known about how their expression is regulated. Using CRISPR/Cas9, we introduced 6 G>A mutations predicted to abolish G4 structure formation into the endogenous G4 motif in K562 cells (Fig. 2c and Additional file 1: Fig. S6a–c). Biophysical analysis by circular dichroism spectroscopy confirmed that a DNA oligonucleotide of the selected G4 sequence had a signature consistent with G4 formation in 100 mM KCl (positive peak ~265 nm, negative peak ~240 nm) [36], which is lost in 100 mM LiCl. By contrast the mutated oligonucleotide exhibited a signature consistent with loss of G4 structure (Fig. 2d). Indeed, in edited cells, we observed a reduction in G4 structure (Fig. 2e–g) and G4-associated loops (Fig. 2e) at this locus in two independent clones. Global G4 levels were unchanged (Additional file 1: Fig. S6d), and more loop loss was seen at the RCA locus compared to the remainder of the genome in the mutants (Additional file 1: Fig. S6e–f). Together, this shows that ViCAR will discriminate between unfolded and folded G4s. One limitation of ViCAR, and other immunoprecipitation-based 3D methods, is the dependency on a target feature to probe looping. In cases where the target feature is not available, it is therefore necessary to independently measure changes in the underlying 3D genome. To address what happens to the 3D landscape in the absence of a G4 in the mutant, we performed HiCAR. In edited cells, we observed a reduction in HiCAR loops at the RCA locus, showing that 3D contacts associated with accessible chromatin are reduced upon loss of a G4 (Fig. 2h–i and Additional file 1: Fig. S7a–b). Furthermore, we noted that G4 mutation can perturb gene expression of nearby complement genes CD55 and CD46 as well as C1orf116, YOD1, EIF2D, and PFKFB2 (Fig. 2j and Additional file 3: Table S2), and perturb RNA Pol II occupancy (Additional file 1: Fig. S7c–d). This exemplifies the utility of ViCAR to identify functional distal regulatory regions and pair them with their target genes.

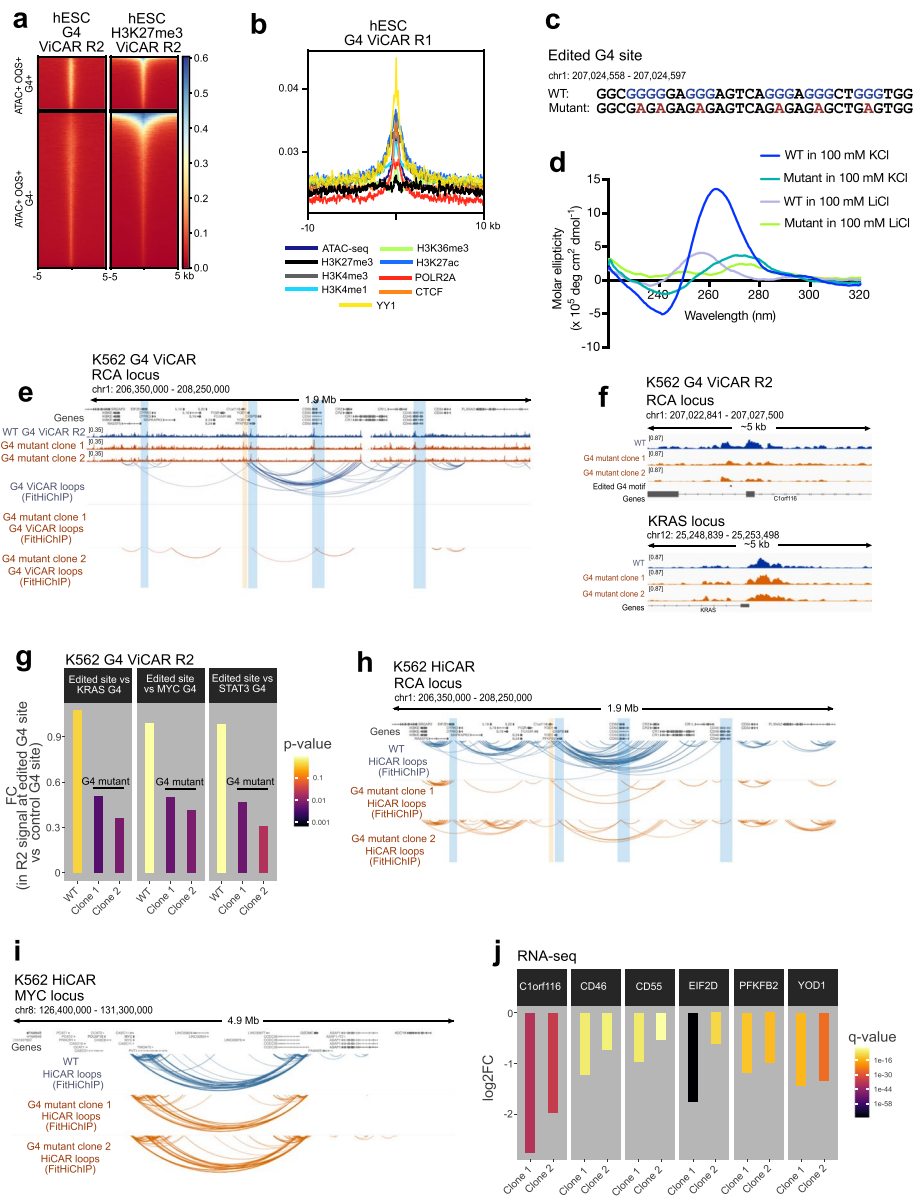


Fig. 2 **a** G4 ViCAR sequencing R2 plotted over G4 ChIP-seq peaks [17] in hESCs (left). H3K27me3 ViCAR sequencing R2 plotted over G4 ChIP-seq peaks is shown for comparison (right). Regions with (G4+) and without (G4-) G4 ChIP peaks in accessible regions (ATAC-seq peaks; ATAC+) that contain sequences capable of forming G4s in vitro (called Observed Quadruplex Sequences, OQS+) are shown. BG4 ViCAR normalized R2 signal is enriched at G4+ sites compared to G4- sites. By contrast, H3K27me3 ViCAR normalized R2 signal mostly accumulates at G4- sites. **b** G4 ViCAR sequencing R1 (i.e., 3D interactions) plotted over ChIP-seq and ATAC-seq peaks. **c** WT and mutant sequence of a G4 oligonucleotide derived from a sequence in an intron of C1orf116. **d** Circular dichroism (CD) spectra of oligonucleotides corresponding to WT and mutant G4 motifs are consistent with a G4 structure in the WT (K⁺-dependent positive peak at ~265 nm and negative peak at ~240 nm) and a loss of G4 structure in the mutant (with a shift towards 280 nm). **e–g** G4 ViCAR data from K562 cells at the edited G4 site in WT and 2 G4 mutant clones. In **e**, the edited G4 site is highlighted by orange shading, and genes affected by the G4 mutation (**j**) are highlighted by blue shading. 2D tracks in **e** show G4 ViCAR R2, and the bottom 3 tracks show loops called by FitHiChIP at 10 kb resolution ($q < 0.01$). **f** G4 ViCAR R2 signal in WT and 2 G4 mutant clones at the edited site. The edited G4 motif is shown by a black bar. **g** Fold change and p values represent R2 signal at the edited site vs R2 signal at 3 control G4 sites (KRAS, MYC, STAT3). HiCAR data from K562 cells at the edited G4 site (**h**) and the unedited MYC locus (**i**) in WT and 2 G4 mutant clones. In **h**, the edited G4 site is highlighted by orange shading, and genes affected by the G4 mutation (**j**) are highlighted by blue shading. Loops were called using FitHiChIP at 10 kb resolution ($q < 0.01$). **j** Expression of selected genes near to the edited G4 site measured by RNA-seq

Conclusions

Here, we introduce ViCAR, which demonstrates several advantages for capturing 3D genome interactions marked by specific epigenetic features. ViCAR shows substantial improvements in sensitivity and significant loop identification compared to other methods. The G4 field to date has relied on indirect correlations to link G4s to 3D genome structure. A major advance is the ability of ViCAR to simultaneously map DNA secondary structures and 3D loops at read-level genome-wide, thus directly demonstrating that they co-occur in the same cell at the same time. ViCAR confirms previously predicted loops and robustly captures G4-3D interactions genome-wide. We anticipate that ViCAR will provide a simple and superior tool to analyze a wide range of factors in 3D genome structure regulation.

Methods

Methods are provided in Additional file 6.

Supplementary Information

The online version contains supplementary material available at <https://doi.org/10.1186/s13059-024-03377-6>.

Additional file 1. Supplementary figures.

Additional file 2: Table S1. ViCAR library statistics.

Additional file 3: Table S2. Differential gene expression analysis (RNA-seq).

Additional file 4: Table S3. Oligonucleotide sequences.

Additional file 5: Table S4. Number of replicates for sequencing experiments.

Additional file 6. Methods [57–64].

Additional file 7. Review history.

Acknowledgements

We thank the Genomic, Flow Cytometry and Research Instrumentation and Cell Services core facilities at the Cancer Research UK Cambridge Institute for technical support.

Peer review information

Ferhat Ay and Wenjing She were the primary editors of this article and managed its editorial process and peer review in collaboration with the rest of the editorial team.

Review history

The review history is available as Additional file 7.

Authors' contributions

S.M.F., D.T., and S.B. conceived the project. S.M.F., S.D., K.H., C.D., S.S., D.T., and S.B. designed the experiments with input from all authors. S.M.F. and C.D. generated ViCAR and CUT&Tag data. K.H. generated RNA-seq data. K.H. and S.M.F. performed CRISPR/Cas9 experiments. Computational analyses were performed by S.D. (ViCAR and RNA-seq), L.M. (CUT&Tag), and L.M. and A.S. (during method development). W.W.I.H. purified pA-Tn5. R.d.C.A.T cultured mESCs. The manuscript was drafted by S.M.F., D.T., and S.B. and reviewed and edited by S.M.F., S.D., K.H., C.D., L.M., W.W.I.H., S.S., D.T., and S.B.

Funding

The Balasubramanian laboratory is supported by Cancer Research UK core (C9545/A19863; SEBINT-2024/100003) and programme award funding (C9681/A29214) and Herchel Smith Funds. S.B. is a Senior Investigator of the Wellcome Trust (209441/Z/17/Z). S.M.F. is also supported by a Leverhulme Trust Early Career Fellowship (ECF-2021–398). S.S. was funded by the UKRI BBSRC Epigenetics Institute Strategic Programme Grant (BBS/E/B/000C0421), a UKRI MRC Rutherford Fund Fellowship (MR/T016787/1), and a Career Progression Fellowship from the Babraham Institute.

Availability of data and materials

Data generated in this study are deposited in NCBI Gene Expression Omnibus (GEO; <https://www.ncbi.nlm.nih.gov/geo/>) with accession code GSE250219 [37]. The following data from the 4DN data portal [38] were used: 4DNEXRI3VAH3 (K562 PLAC-seq) [24, 39], 4DNESI7DEJTM (K562 in situ Hi-C) [29, 40]. The following data from Gene Expression Omnibus were used: GSE162819 (hESC HiCAR) [5, 41], GSE150907 (hiPSC H3K27me3 HiChIP and mESC H3K27me3 HiChIP) [23, 42], GSM5658773 (mESC H3K27me3 ChIP-seq) [26, 43], GSE186011 (GM12878 H3K27ac HiCuT) [6, 44], GSE161531 (hESC G4 ChIP-seq and hESC H3K27me3 ChIP-seq) [17, 45], GSE162299 (K562 G4 ChIP-seq) [46, 47]. The following ENCODE datasets were used: ENCF927FVH (hESC H3K27me3 ChIP-seq) [48, 49], ENCF368LWM (hESC CTCF ChIP-seq) [50, 51],

ENCF5991HW (hESC H3K36me3 ChIP-seq) [48, 52], ENCF162HPV (hESC H3K27ac ChIP-seq) [50, 53], ENCF480QNT (hESC H3K4me1 ChIP-seq) [50, 51], ENCF120KQK (hESC H3K4me3 ChIP-seq) [50, 51], ENCSR000AKC (GM12878 H3K27ac ChIP-seq) [50, 51], ENCSR000BKD (hESC YY1 ChIP-seq) [53, 54]. Code is available on GitHub [55] and Zenodo [56] under a Creative Commons Zero v1.0 Universal License.

Declarations

Ethics approval and consent to participate

Work with hESCs was authorized by the Steering Committee for the UK Stem Cell Bank and for Use of Stem Cells (MRC).

Consent for publication

Not applicable.

Competing interests

S.B. is a founder and shareholder of Biomodal Ltd, GenomeTx, and RNAvate Ltd. L.M. is a consultant for Inflex Ltd. S.S. is a co-founder and shareholder of Enhanc3D Genomics Ltd.

Received: 11 March 2024 Accepted: 25 August 2024

Published online: 03 September 2024

References

- Lieberman-Aiden E, Van Berkum NL, Williams L, Imakaev M, Ragozcy T, Telling A, et al. Comprehensive mapping of long-range interactions reveals folding principles of the human genome. *Science*. 1979;2009(326):289–93.
- Tolhuis B, Palstra R-J, Splinter E, Grosveld F, De Laat W. Looping and interaction between hypersensitive sites in the active beta-globin locus. *Mol Cell*. 2002;10:1453–65.
- Schoenfelder S, Furlan-Magaril M, Mifsud B, Tavares-Cadete F, Sugar R, Javierre BM, et al. The pluripotent regulatory circuitry connecting promoters to their long-range interacting elements. *Genome Res*. 2015;25:582–97.
- Mifsud B, Tavares-Cadete F, Young AN, Sugar R, Schoenfelder S, Ferreira L, et al. Mapping long-range promoter contacts in human cells with high-resolution capture Hi-C. *Nat Genet*. 2015;47:598–606.
- Wei X, Xiang Y, Peters DT, Marius C, Sun T, Shan R, et al. HiCAR is a robust and sensitive method to analyze open-chromatin-associated genome organization. *Mol Cell*. 2022;82:1225–1238.e6.
- Sati S, Jones P, Kim HS, Zhou LA, Rapp-Reyes E, Leung TH. HiCuT: an efficient and low input method to identify protein-directed chromatin interactions. *PLoS Genet*. 2022;18:e1010121.
- Fang R, Yu M, Li G, Chee S, Liu T, Schmitt AD, et al. Mapping of long-range chromatin interactions by proximity ligation-assisted ChIP-seq. *Cell Res*. 2016;26:1345–8.
- Mumbach MR, Rubin AJ, Flynn RA, Dai C, Khavari PA, Greenleaf WJ, et al. HiChIP: efficient and sensitive analysis of protein-directed genome architecture. *Nat Methods*. 2016;13:919–22.
- Robinson J, Raguseo F, Nuccio SP, Liano D, Di Antonio M. DNA G-quadruplex structures: more than simple road-blocks to transcription? *Nucleic Acids Res*. 2021;49:8419–31.
- Varshney D, Spiegel J, Zyner K, Tannahill D, Balasubramanian S. The regulation and functions of DNA and RNA G-quadruplexes. *Nat Rev Mol Cell Biol*. 2020;21:459–74.
- Hänsel-Hertsch R, Beraldi D, Lensing SV, Marsico G, Zyner K, Parry A, et al. G-quadruplex structures mark human regulatory chromatin. *Nat Genet*. 2016;48:1267–72.
- Li C, Wang H, Yin Z, Fang P, Xiao R, Xiang Y, et al. Ligand-induced native G-quadruplex stabilization impairs transcription initiation. *Genome Res*. 2021;31:1546–60.
- Hui WWI, Simeone A, Zyner KG, Tannahill D, Balasubramanian S. Single-cell mapping of DNA G-quadruplex structures in human cancer cells. *Sci Rep*. 2021;11:23641.
- Lyu J, Shao R, Kwong Yung PY, Elsässer SJ. Genome-wide mapping of G-quadruplex structures with CUT&Tag. *Nucleic Acids Res*. 2022;50:E13.
- Galli S, Melidis L, Flynn SM, Varshney D, Simeone A, Spiegel J, et al. DNA G-quadruplex recognition in vitro and in live cells by a structure-specific nanobody. *J Am Chem Soc*. 2022;144:23096–103.
- Yu Z, Spiegel J, Melidis L, Hui WWI, Zhang X, Radzevičius A, et al. Chem-map profiles drug binding to chromatin in cells. *Nat Biotechnol*. 2023;41:1265–71.
- Zyner KG, Simeone A, Flynn SM, Doyle C, Marsico G, Adhikari S, et al. G-quadruplex DNA structures in human stem cells and differentiation. *Nat Commun*. 2022;13:142.
- Li L, Williams P, Ren W, Wang MY, Gao Z, Miao W, et al. YY1 interacts with guanine quadruplexes to regulate DNA looping and gene expression. *Nat Chem Biol*. 2021;17:161–8.
- Yuan J, He X, Wang Y. G-quadruplex DNA contributes to RNA polymerase II-mediated 3D chromatin architecture. *Nucleic Acids Res*. 2023;51:8434–46.
- Wulfridge P, Yan Q, Rell N, Doherty J, Jacobson S, Offley S, et al. G-quadruplexes associated with R-loops promote CTCF binding. *Mol Cell*. 2023;83:3064–79.
- Hänsel-Hertsch R, Simeone A, Shea A, Hui WWI, Zyner KG, Marsico G, et al. Landscape of G-quadruplex DNA structural regions in breast cancer. *Nat Genet*. 2020;52:878–83.
- Kaya-Okur HS, Wu SJ, Codomo CA, Pledger ES, Bryson TD, Henikoff JG, et al. CUT&Tag for efficient epigenomic profiling of small samples and single cells. *Nat Commun*. 2019;10:1930.
- Kraft K, Yost K, Murphy S, Magg A, Long Y, Corces R, et al. Polycomb-mediated genome architecture enables long-range spreading of H3K27 methylation. *Proc Natl Acad Sci U S A*. 2020;119:e2201883119.

24. Calandrelli R, Wen X, Charles Richard JL, Luo Z, Nguyen TC, Chen CJ, et al. Genome-wide analysis of the interplay between chromatin-associated RNA and 3D genome organization in human cells. *Nat Commun.* 2023;14:6519.
25. Cruz-Molina S, Respuela P, Tebartz C, Kolovos P, Nikolic M, Fueyo R, et al. PRC2 facilitates the regulatory topology required for poised enhancer function during pluripotent stem cell differentiation. *Cell Stem Cell.* 2017;20:689–705. e9.
26. Alfert A, Walter C, Moreno N, Melcher V, Graf M, Hotfilder M, et al. Smarcb1 loss results in a deregulation of esBAF binding and impacts the expression of neurodevelopmental genes. *Cells.* 2022;11:1354.
27. Chovanec P, Collier AJ, Krueger C, Várnai C, Semprich CI, Schoenfelder S, et al. Widespread reorganisation of pluripotent factor binding and gene regulatory interactions between human pluripotent states. *Nat Commun.* 2021;12:2098.
28. Bhattacharyya S, Chandra V, Vijayanand P, Ay F. Identification of significant chromatin contacts from HiChIP data by FitHiChIP. *Nat Commun.* 2019;10:4221.
29. Rao SSP, Huntley MH, Durand NC, Stamenova EK, Bochkov ID, Robinson JT, et al. A 3D map of the human genome at kilobase resolution reveals principles of chromatin looping. *Cell.* 2014;159:1665–80.
30. Schuijers J, Manteiga JC, Weintraub AS, Day DS, Zamudio AV, Hnisz D, et al. Transcriptional dysregulation of MYC reveals common enhancer-docking mechanism. *Cell Rep.* 2018;23:349–60.
31. Fulco CP, Munschauer M, Anyoha R, Munson G, Grossman SR, Perez EM, et al. Systematic mapping of functional enhancer-promoter connections with CRISPR interference. *Science.* 1979;2016(354):769–73.
32. Guc D, Canpinar H, Kucukakcu C, Kansu E. Expression of complement regulatory proteins CR1, DAF, MCP and CD59 in haematological malignancies. *Eur J Haematol.* 2000;64:3–9.
33. Fishelson Z, Donin N, Zell S, Schultz S, Kirschfink M. Obstacles to cancer immunotherapy: expression of membrane complement regulatory proteins (mCRPs) in tumors. *Mol Immunol.* 2003;40:109–23.
34. Dho SH, Lim JC, Kim LK. Beyond the role of CD55 as a complement component. *Immune Netw.* 2018;18:e11.
35. Liszewski MK, Atkinson JP. Membrane cofactor protein (MCP; CD46): deficiency states and pathogen connections. *Curr Opin Immunol.* 2021;72:126–34.
36. Balagurumoorthy P, Brahmachari SK, Mohanty D, Bansal M, Sasisekharan V. Hairpin and parallel quartet structures for telomeric sequences. *Nucleic Acids Res.* 1992;20:4061–7.
37. Flynn SM, Dhir S, Herka K, Doyle C, Melidis L, Simeone A, et al. Improved simultaneous mapping of epigenetic features and 3D chromatin structure via ViCAR. *GSE250219.* Gene Expression Omnibus. 2024. <https://www.ncbi.nlm.nih.gov/geo/query/acc.cgi?acc=GSE250219>.
38. Reiff SB, Schroeder AJ, Kirli K, Cosolo A, Bakker C, Lee S, et al. The 4D nucleome data portal as a resource for searching and visualizing curated nucleomics data. *Nat Commun.* 2022;13:6561.
39. Proximity ligation with ChIP experiment PLAC-seq against H3K4me3 on K562 (tier 2). 2021. <https://data.4dnucleome.org/experiments-chiapet/4DNEXR3VAH3/>.
40. In situ Hi-C on K562 with Mbol and bio-dATP (higher crosslinker concentration). 2017. <https://data.4dnucleome.org/experiment-set-replicates/4DNES17DEJTM/>.
41. Wei X, Xiang Y, Peters DT, Marius C, Sun T, Shan R, et al. HiCAR is a robust and sensitive method to analyze open-chromatin-associated genome organization. *GSE162819.* Gene Expression Omnibus. 2022. <https://www.ncbi.nlm.nih.gov/geo/query/acc.cgi?acc=GSE162819>.
42. Kraft K, Yost K, Murphy S, Magg A, Long Y, Corces R, et al. Polycomb-mediated genome architecture enables long-range spreading of H3K27 methylation. *GSE150907.* Gene Expression Omnibus. 2022. <https://www.ncbi.nlm.nih.gov/geo/query/acc.cgi?acc=GSE150907>.
43. Alfert A, Walter C, Moreno N, Melcher V, Graf M, Hotfilder M, et al. Smarcb1 loss results in a deregulation of esBAF binding and impacts the expression of neurodevelopmental genes. *GSM5658773.* Gene Expression Omnibus. 2022. <https://www.ncbi.nlm.nih.gov/geo/query/acc.cgi?acc=GSM5658773>.
44. Sati S, Jones P, Kim HS, Zhou LA, Rapp-Reyes E, Leung TH. HiCuT: an efficient and low input method to identify protein-directed chromatin interactions. *GSE186011.* Gene Expression Omnibus. 2021. <https://www.ncbi.nlm.nih.gov/geo/query/acc.cgi?acc=GSE186011>.
45. Zyner KG, Simeone A, Flynn SM, Doyle C, Marsico G, Adhikari S, et al. G-quadruplex DNA structures in human stem cells and differentiation. *GSE161531.* Gene Expression Omnibus. 2021. <https://www.ncbi.nlm.nih.gov/geo/query/acc.cgi?acc=GSE161531>.
46. Shen J, Varshney D, Simeone A, Zhang X, Adhikari S, Tannahill D, et al. Promoter G-quadruplex folding precedes transcription and is controlled by chromatin. *Genome Biol.* 2021;22:143.
47. Shen J, Varshney D, Simeone A, Zhang X, Adhikari S, Tannahill D, et al. Promoter G-quadruplex folding precedes transcription and is controlled by chromatin. *GSE162299.* Gene Expression Omnibus. 2021. <https://www.ncbi.nlm.nih.gov/geo/query/acc.cgi?acc=GSE162299>.
48. Bernstein BE, Stamatoyannopoulos JA, Costello JF, Ren B, Milosavljevic A, Meissner A, et al. The NIH roadmap epigenomics mapping consortium. *Nat Biotechnol.* 2010;28:1045–8.
49. Bernstein BE, Stamatoyannopoulos JA, Costello JF, Ren B, Milosavljevic A, Meissner A, et al. The NIH roadmap epigenomics mapping consortium. *GSE17312.* Gene Expression Omnibus. 2021. <https://www.ncbi.nlm.nih.gov/geo/query/acc.cgi?acc=GSE17312>.
50. ENCODE Project Consortium. An integrated encyclopedia of DNA elements in the human genome. *Nature.* 2012;489:57–74.
51. ENCODE Project Consortium. Consortium. An integrated encyclopedia of DNA elements in the human genome. *GSE29611.* Gene Expression Omnibus. 2021. <https://www.ncbi.nlm.nih.gov/geo/query/acc.cgi?acc=GSE29611>.
52. Bernstein BE, Stamatoyannopoulos JA, Costello JF, Ren B, Milosavljevic A, Meissner A, et al. The NIH roadmap epigenomics mapping consortium. *GSE16256.* Gene Expression Omnibus. 2021. <https://www.ncbi.nlm.nih.gov/geo/query/acc.cgi?acc=GSE16256>.
53. Gertz J, Savic D, Varley KE, Partridge EC, Safi A, Jain P, et al. Distinct properties of cell-type-specific and shared transcription factor binding sites. *Mol Cell.* 2013;52:25–36.

54. Gertz J, Savic D, Varley KE, Partridge EC, Safi A, Jain P, et al. Distinct properties of cell-type-specific and shared transcription factor binding sites. GSE32465. Gene Expression Omnibus. 2021. <https://www.ncbi.nlm.nih.gov/geo/query/acc.cgi?acc=GSE32465>.
55. Flynn SM, Dhir S, Herka K, Doyle C, Melidis L, Simeone A, et al. VICAR. Github. 2024. <https://github.com/sblab-informatics/VICAR>.
56. Flynn SM, Dhir S, Herka K, Doyle C, Melidis L, Simeone A, et al. VICAR analysis pipeline. 2024. Zenodo. <https://doi.org/10.5281/zenodo.13309627>.
57. Fujiwara Y, Tanno Y, Sugishita H, Kishi Y, Makino Y, Okada Y. Preparation of optimized concanavalin A-conjugated Dynabeads® magnetic beads for CUT&Tag. PLoS ONE. 2021;16:e0259846.
58. Li H, Durbin R. Fast and accurate long-read alignment with Burrows-Wheeler transform. Bioinformatics. 2010;26:589–95.
59. Open2C, Abdennur N, Fudenberg G, Flyamer IM, Galitsyna AA, Goloborodko A, et al. Pairtools: from sequencing data to chromosome contacts. PLoS Comput Biol. 2024;20(5):e1012164.
60. Durand NC, Robinson JT, Shamim MS, Machol I, Mesirov JP, Lander ES, et al. Juicebox provides a visualization system for Hi-C contact maps with unlimited zoom. Cell Syst. 2016;3:99–101.
61. Li D, Hsu S, Purushotham D, Sears RL, Wang T. WashU epigenome browser update 2019. Nucleic Acids Res. 2019;47:W158–65.
62. Ramírez F, Ryan DP, Grüning B, Bhardwaj V, Kilpert F, Richter AS, et al. deepTools2: a next generation web server for deep-sequencing data analysis. Nucleic Acids Res. 2016;44:W160–5.
63. Ran FA, Hsu PD, Wright J, Agarwala V, Scott DA, Zhang F. Genome engineering using the CRISPR-Cas9 system. Nat Protoc. 2013;8:2281–308.
64. Handyside AH, O'Neill GT, Jones M, Hooper ML. Use of BRL-conditioned medium in combination with feeder layers to isolate a diploid embryonal stem cell line. Roux Arch Dev Biol. 1989;198:48–56.

Publisher's Note

Springer Nature remains neutral with regard to jurisdictional claims in published maps and institutional affiliations.